Available on CMS information server

CMS NOTE 2006/069

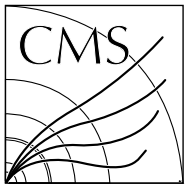

The Compact Muon Solenoid Experiment

CMS Note

Mailing address: CMS CERN, CH-1211 GENEVA 23, Switzerland

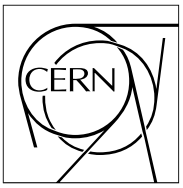

May 17, 2006

Jet Triggers and Dijet Mass

Selda Esen

Cukurova University, Adana, Turkey

Visitor at Fermilab, Batavia, IL, USA

Robert M. Harris

Fermilab, Batavia, IL, USA

Abstract

We propose single jet triggers for CMS and simulate an analysis of the dijet mass distribution based on these triggers. A full trigger table for single jets is developed, including thresholds and prescales at L1 and HLT. The evolution of the table with instantaneous luminosity is presented, and the rates expected from the trigger are estimated. We present an analysis of the QCD dijet mass distribution that would result from taking data with this trigger. For three different samples of data corresponding to 100 pb^{-1}, 1 fb^{-1}, and 10 fb^{-1}we estimate the expected statistical and systematic uncertainty on the cross section versus dijet mass.

1 Introduction

The measurement of the dijet mass spectrum at CMS requires a jet trigger. In this note we propose a jet trigger table for CMS based on the experience of triggering on jets at the Tevatron. Using this trigger we estimate the resulting dijet mass spectrum and its statistical and systematic uncertainty.

We have been driven by the needs of the dijet analysis which requires measurement of the dijet mass spectrum over a wide range of mass. The measurement of lower dijet mass values requires special trigger considerations. While measurement of the highest dijet mass values is critical in searches for new physics, triggering on these events is simple. Measurement of relatively low dijet masses is important because it anchors the distributions in the well understood dijet mass regions previously explored by the Tevatron and understood to be dominated by QCD dijet production. The measurement at low mass allows us to constrain the value of the QCD background and conduct realistic searches for new physics.

2 Data Sample and Jet Reconstruction

All plots in this note are made from a sample of QCD jet events generated with Pythia, passed through the full CMS detector simulation, and reconstructed with the ORCA [1] reconstruction package. A total of 210,000 events were used, from 21 samples each consisting of 10,000 events sub-samples in contiguous intervals in generator level of p_T spanning from 0 to 4000 GeV: 0-15, 15-20, 20-30, 30-50, 50-80, 80-120, 120-170, 170-230, 230-300, 300-380, 380-470, 470-600, 600-800, 800-1000, 1000-1400, 1400-1800, 1800-2200, 2200-2600, 2600-3000, 3000-3500 and 3500-4000. Projective towers of calorimeter energy deposits (EcalPlusHcalTowers) were reconstructed with the default CMS algorithm which had a cut at 0.5 GeV on the energy in each HCAL compartment. Offline jets were reconstructed with the default CMS algorithm [2]: iterative cone algorithm, a cone size of $R = 0.5$, no seed threshold, 0.5 GeV E_T tower threshold, and E-scheme method of constructing jet four vectors. Jets from the High Level Trigger (HLT) are assumed to be the same as offline jets, since the HLT will run the offline software for jet reconstruction. Jets from the L1 trigger are a square array of trigger towers (like EcalPlusHcalTowers), 12 towers in η by 12 towers in ϕ. All reconstructed offline jets with $p_T > 10$ GeV were written to a root tree [3], along with a single multiplicative correction factor for the offline jet Lorentz vector.

The jet correction is designed to give a Lorentz vector from the particles in a jet cone of radius $R = 0.5$ before pileup. The correction depends on reconstructed jet $p_{\rm T}$ and η. For jets in the region $|\eta| < 1$ on average a reconstructed $p_{\rm T}$ of 75 GeV was corrected by 33% to give 100 GeV, a $p_{\rm T}$ of 430 GeV by 16% to give 500 GeV, and a $p_{\rm T}$ of 2.8 TeV by 7% to give 3.0 TeV corrected jet $p_{\rm T}$. The correction as a function of jet $p_{\rm T}$ is shown in Fig. 1 for three different values of jet $|\eta|$ within the barrel calorimeter. The variation of the jet correction with $|\eta|$ for a fixed $p_{\rm T}$ was dominated by the simulated electronic noise which contributed 8.5 GeV of energy to the jet on average in the barrel [4]. In addition to correcting for calorimeter non-linearities, the correction on average removes noise above the threshold on the energy in each calorimeter compartment. As a consequence, the jet correction is sensitive to the noise threshold, and the correction used here is only applicable for jets reconstructed from EcalPlusHcalTowers with a 0.5 GeV energy threshold on each HCAL compartment.

All L1 jets were written to a root tree [5]. Analogous to offline jets, a multiplicative correction factor was developed [6] for the L1 jet Lorentz vector that corrects the reconstructed

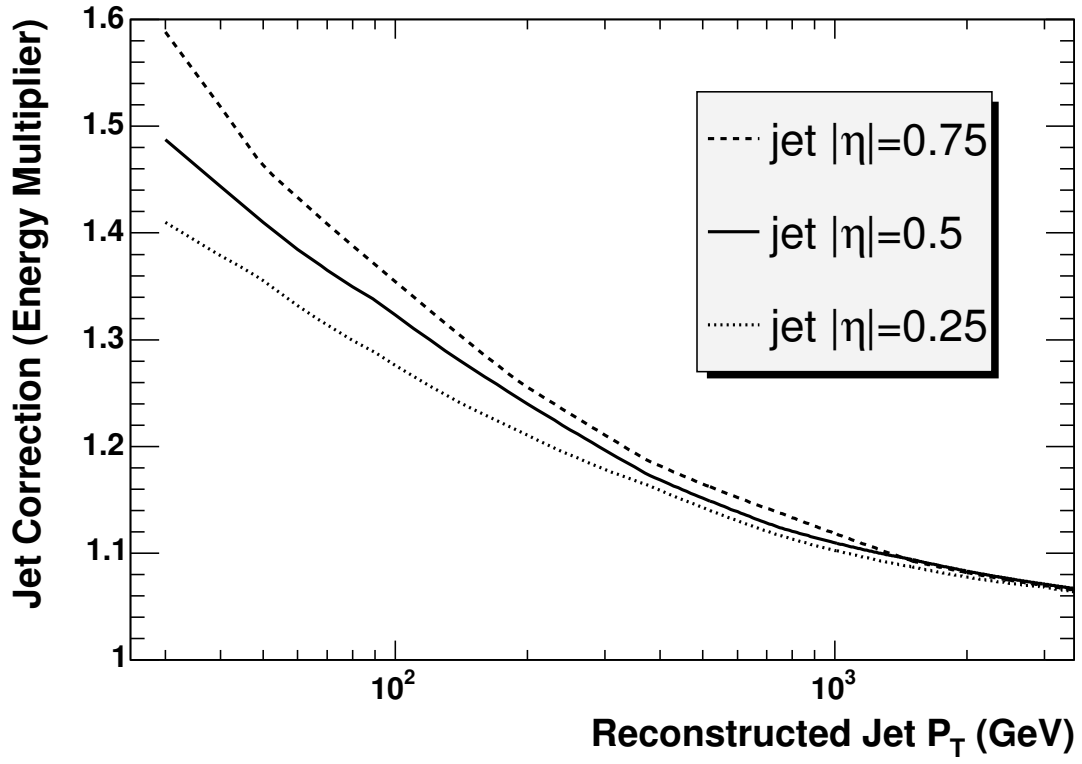

Figure 1: The offline jet correction as a function of reconstructed jet p_{T} for three values of jet $|\eta|$. The correction is only applicable to the algorithm discussed in the text.

L1 jets back to a matched jet of particles in a cone of radius $R = 0.5$ before pileup. The sample consists of a mixture of QCD jet events and minimum bias events corresponding to the anticipated number of multiple interactions for a luminosity of 2×10^{33} cm^{-2} s^{-1}. Each sub-sample has a weight corresponding to the generated cross section per event for that sub-sample. The weights vary significantly from sample to sample, ranging from 5.5×10^{6} pb for the 0-15 sample to 9.7×10^{-9} pb for the 3500-4000 sample. When making a histogram all events from each sub-sample are used along with their corresponding weight, and all errors are calculated taking into account the weights.

3 Single Jet Triggers

In this section we discuss the trigger table that will be used for subsequent analysis. In section 3.1 we propose the trigger table and in section 3.2 we discuss the table's design at the lowest luminosity and its subsequent evolution with increasing luminosity over a time of years.

3.1 Trigger Table Proposal

Here we propose the single jet trigger tables for CMS. We will define the trigger paths from L1 through HLT. This includes reasonable thresholds, prescales, estimates of the resulting rates at L1 and HLT, and evolution of the trigger table with increasing luminosity. To measure jet spectra down to low jet E_T and dijet mass requires multiple triggers, of roughly equal

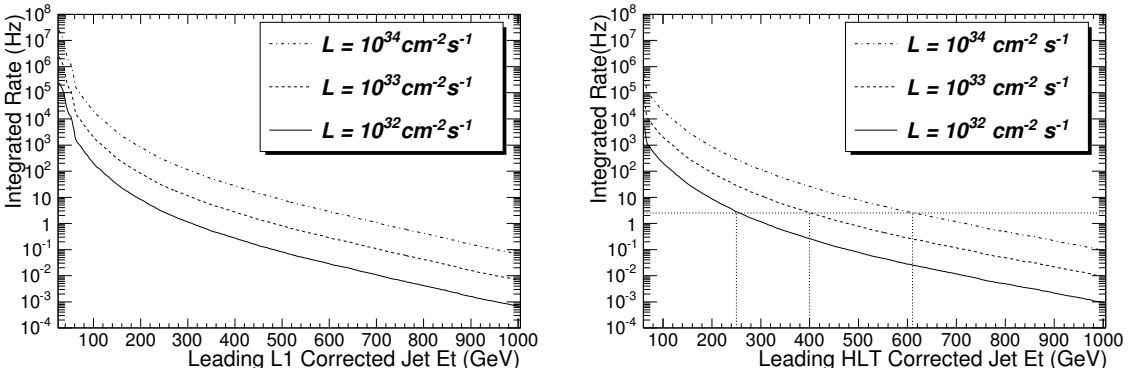

Figure 2: The integrated trigger rates at L1 (left) and HLT (right) above the E_T thresholds for the highest E_T jet is plotted versus the E_T threshold for three luminosity scenarios: $\mathcal{L} = 10^{32}\ \mathrm{cm}^{-2}\,\mathrm{s}^{-1}$ (solid) , and $\mathcal{L} = 10^{33}\ \mathrm{cm}^{-2}\,\mathrm{s}^{-1}$ (dashed), and $\mathcal{L} = 10^{34}\ \mathrm{cm}^{-2}\,\mathrm{s}^{-1}$ (dot-dashed). HLT thresholds that give 2.5 Hz are shown by vertical dotted lines.

total rate, and with appropriately chosen E_T thresholds and prescales. The trigger rate will depend on the luminosity. We consider four scenarios for the instantaneous luminosity of the LHC:

1. $\mathcal{L} = 10^{32}\ \mathrm{cm}^{-2}\,\mathrm{s}^{-1}$
2. $\mathcal{L} = 10^{33}\ \mathrm{cm}^{-2}\,\mathrm{s}^{-1}$
3. $\mathcal{L} = 2 \times 10^{33}\ \mathrm{cm}^{-2}\,\mathrm{s}^{-1}$
4. $\mathcal{L} = 10^{34}\ \mathrm{cm}^{-2}\,\mathrm{s}^{-1}$

In figure 2 we show estimates of the L1 and HLT single jet trigger rates vs. corrected jet E_T for three of these scenarios. In table 1 we show the single jet trigger paths from L1 to HLT including thresholds, prescales and estimates of the rates. The main constraining factor for triggering on jets is the allowed HLT bandwidth. For luminosity scenario 1, 2 and 4 the highest E_T threshold at HLT was chosen to give a rate of roughly 2.5 Hz, as illustrated in figure 2, so that four triggers would saturate an allowed jet rate of roughly 10 Hz at HLT. The highest E_T threshold in each scenario is not prescaled. Lower thresholds are prescaled and are chosen at roughly half the E_T of the next highest threshold. This allows reasonable statistics in the overlap between the two samples, necessary for measuring trigger efficiencies and producing a continuous jet spectrum. Note that the total L1 jet rate required is around 0.3 KHz, within the alloted L1 total bandwidth for jets. Since we are limited by HLT, not L1, for each trigger path the L1 thresholds are chosen low enough to have a L1 trigger efficiency of more than 95% at the corresponding HLT threshold in the path, as shown in Figure 3. This strategy utilizes ten times more bandwidth at L1 than at HLT to insure that all of the resulting HLT sample has high enough trigger efficiency to be useful for analysis.

3.2 Discussion of Trigger Table

Here we go through table 1, discuss how it was designed, and make a few recommendations for trigger operations from a physics analysis perspective.

Path	L1				HLT	
	E_T Cut (GeV)	Unpres. Rate (KHz)	Prescale (N)	Presc. Rate (KHz)	E_T Cut GeV)	Rate (Hz)
Single Jet Triggers in Scenario 1: $\mathcal{L} = 10^{32}\ \mathrm{cm}^{-2}\,\mathrm{s}^{-1}$						
High	140	0.044	1	0.044	250	2.8
Med	60	3.9	40	0.097	120	2.4
Low	25	2.9×10^2	2,000	0.146	60	2.8
Single Jet Triggers in Scenario 2: $\mathcal{L} = 10^{33}\ \mathrm{cm}^{-2}\,\mathrm{s}^{-1}$						
Ultra	270	0.019	1	0.019	400	2.6
High	140	0.44	10	0.044	250	2.8
Med	60	39	400	0.097	120	2.4
Low	25	2.9×10^3	20,000	0.146	60	2.8
Single Jet Triggers in Scenario 3: $\mathcal{L} = 2 \times 10^{33}\ \mathrm{cm}^{-2}\,\mathrm{s}^{-1}$						
Ultra	270	0.038	1	0.038	400	5.2
High	140	0.88	20	0.044	250	2.8
Med	60	78	800	0.097	120	2.4
Low	25	5.8×10^3	40,000	0.146	60	2.8
Single Jet Triggers in Scenario 4: $\mathcal{L} = 10^{34}\ \mathrm{cm}^{-2}\,\mathrm{s}^{-1}$						
Super	450	0.014	1	0.014	600	2.8
Ultra	270	0.19	10	0.019	400	2.6
High	140	4.4	100	0.044	250	2.8
Med	60	3.9×10^2	4,000	0.097	120	2.4
Low	25	2.9×10^4	200,000	0.146	60	2.8

Table 1: Single jet trigger table showing path names, trigger thresholds in corrected E_T, prescales, and estimated rates at L1 and HLT for four different luminosity scenarios.

3.2.1 Design of First Trigger Table

First, we assume the jet trigger is commissioned at an LHC luminosity of $\mathcal{L} = 10^{32}\ \mathrm{cm}^{-2}\,\mathrm{s}^{-1}$, and the jet E_T thresholds are chosen to saturate the allowed HLT bandwidth for jets. If the luminosity is different, other thresholds may be chosen, but we recommend at least three to supply both a large E_T range and have sufficient triggers to measure efficiencies and check one trigger against the other. Clearly our trigger strategy is an example, to demonstrate the principle, and actual threshold numbers themselves will be determined when we have data. The triggers work in a path that start at a specific L1 trigger and flow to a specific HLT trigger: for example the HLT trigger in the *High* path only looks at events that have passed the L1 trigger in the *High* path.

We started with the *High* path by defining the HLT E_T threshold of 250 GeV, which satisfies our rate requirement of roughly 2.5 Hz for this luminosity. The L1 trigger threshold for the *High* path is then chosen at 140 GeV, low enough so the HLT trigger is fully efficient at HLT E_T of 250 GeV, as shown in figure 3. This L1 choice allows subsequent analysis to make full use of the HLT bandwidth, which is more precious than L1 bandwidth for jet analysis. This is better than the situation at CDF, where the L1, L2 and L3 triggers within a path had to be spaced closer and there was always some inefficiency in a lower level trigger when the next level started to turn on. The HLT trigger in the *Med* path is then chosen at an E_T threshold

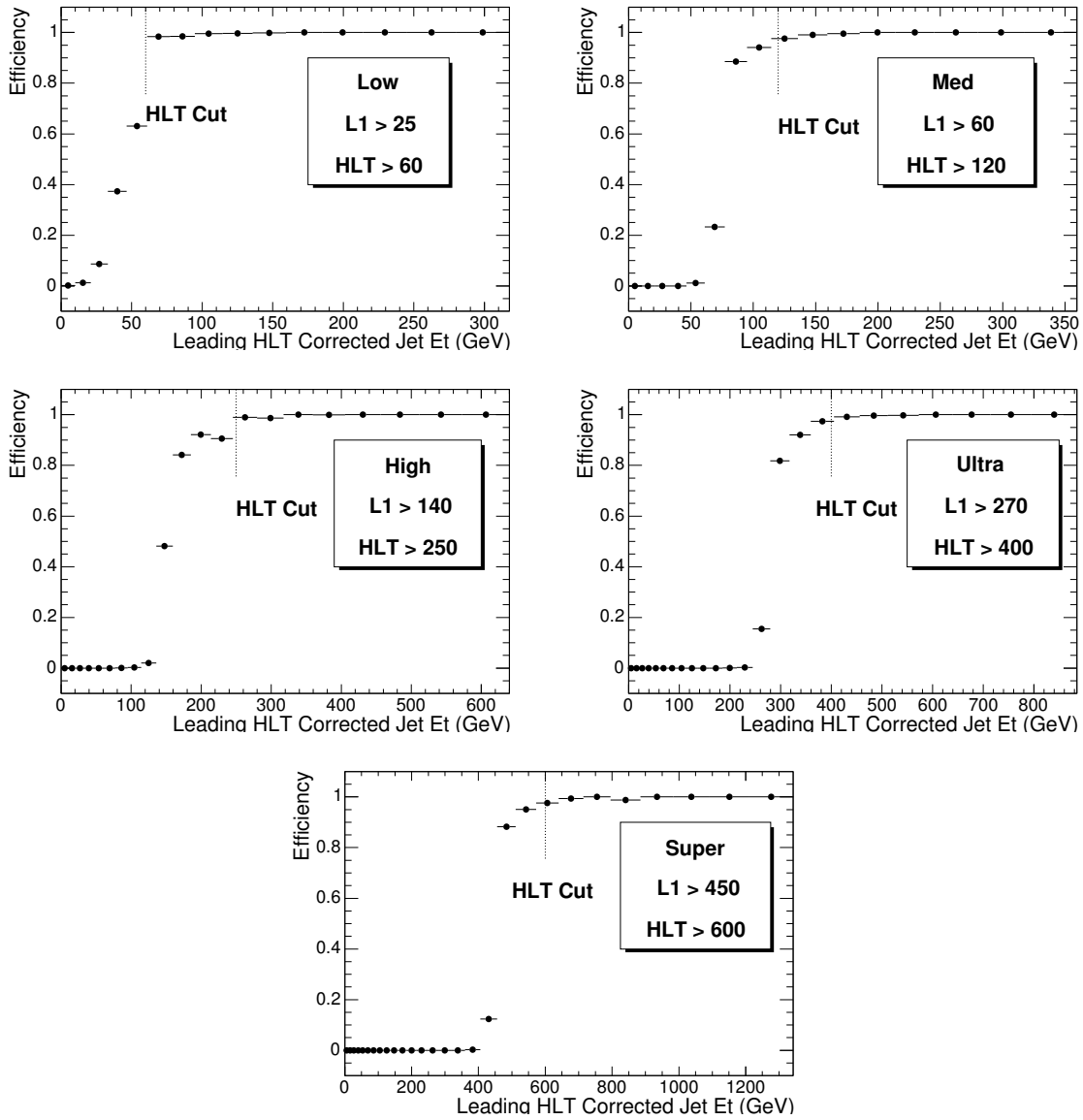

Figure 3: The efficiency for passing the L1 jet trigger is shown as a function of HLT corrected jet E_T for each of the trigger paths shown in table 1. The L1 thresholds were chosen to give an efficiency of greater than 95% at the corresponding HLT threshold.

of 120 GeV, roughly half the value of the HLT threshold in the *High* path, and again the L1 threshold of 60 GeV is chosen so that HLT threshold of 120 GeV is fully efficient. Since the unprescaled rate for this trigger would be too high, flooding the HLT bandwidth with a total rate of roughly 100 Hz, we introduce a prescale at L1, reducing the L1 rate by a factor of 40. Since the *Med* path requires the L1 trigger before it considers the HLT trigger, this also reduces the HLT rate by a factor of 40, and we do not take any L1 rate that we do not intend to use at HLT. Similarly, for the *Low* path, we get the HLT threshold, 60 GeV, from half the value of the HLT threshold in the *Med* path, 120 GeV, and find the value of the L1 threshold, 25 GeV, which gives full efficiency for the HLT threshold, 60 GeV, and then increase the prescale at L1 to a value, 2000, which keeps the total rate coming out of that path at HLT at roughly 2.5

Hz.

That is how we designed the trigger table for the lowest luminosity, which is the most important table, because all subsequent tables will inherit its thresholds to preserve continuity of analysis.

3.2.2 Evolution of Trigger Table

Table 1 illustrates a trigger strategy to maintain the continuity of jet analysis as the luminosity increases over a time span of years. The most important feature is that each luminosity scenario maintains the thresholds introduced in the previous scenario, allowing combination of trigger samples over time. For the prescaled thresholds, we may increase the prescales, either in discrete steps or dynamically, to maintain the allowed HLT rate with increasing luminosity. However, to maintain maximum sensitivity to new physics, the highest E_T threshold must never be prescaled.

Specifically, when the luminosity increases by a factor of 10, we assume that a new threshold at higher E_T must be introduced, or we will break the bandwidth budget at HLT. So when the luminosity increases from $\mathcal{L} = 10^{32}\ \mathrm{cm}^{-2}\,\mathrm{s}^{-1}$ to $\mathcal{L} = 10^{33}\ \mathrm{cm}^{-2}\,\mathrm{s}^{-1}$, we introduce the new unprescaled trigger path *Ultra*, and simply raise by a factor of 10 the L1 prescales in the old trigger paths *High*, *Med*, and *Low*. The new unprescaled path *Ultra* allows us to continue the search for new physics at these higher luminosities, and the new prescales give us the same rate in the old trigger paths as before, which are still needed for the ongoing analysis of the QCD background in the presence of changing jet response with evolving detector conditions. The new trigger path *Ultra* will need to be studied, its efficiency measured and the safe value of various cuts for that trigger introduced, but this is the price we must pay to accommodate the jump in luminosity. The efficiency of any analysis cuts for *High*, *Med*, and *Low* may drift a little with time, but we should be able to trace those drifts to changing detector conditions, and we should still be able to combine samples within the same path across the years. However, when the luminosity increases by only a factor of 2 from $\mathcal{L} = 10^{33}\ \mathrm{cm}^{-2}\,\mathrm{s}^{-1}$ to $\mathcal{L} = 2\times10^{33}\ \mathrm{cm}^{-2}\,\mathrm{s}^{-1}$, we double the prescales on the prescaled triggers but don't change either the threshold or the prescale of the highest E_T trigger labeled Ultra. This allows us to maintain stability of the single jet trigger thresholds, and analyses that depend on them, with only modest increases in the total rate for single jets. We wait until the bigger luminosity jump from $\mathcal{L} = 2\times10^{33}\ \mathrm{cm}^{-2}\,\mathrm{s}^{-1}$ to $\mathcal{L} = 10^{34}\ \mathrm{cm}^{-2}\,\mathrm{s}^{-1}$, to again introduce a new path *Super* which then requires a new analysis of this increased threshold. Notice that our emphasis is on providing as much stability as possible to the trigger conditions that greatly affect the subsequent physics analysis. We only introduce new thresholds, we never change the old thresholds. Further, whenever we have a choice between introducing new thresholds or changing prescales, we always change prescales, so as to provide stability for analysis. Relative prescales can always be checked and understood by comparing the rate from the prescaled trigger to the rate from the other jet triggers.

To commission the calorimeters, or perform a one-time jet study, it may be desirable to have more jets. If we want to write more than roughly 10 Hz of single jets at HLT, we recommend using the thresholds in Table 1, or whatever thresholds are eventually chosen for the single jet trigger, but lowering the prescales to obtain more jets at low E_T. This is preferable to moving the threshold for the unprescaled trigger, or any of the triggers, and ending up with a special trigger that is only applicable for a given running period and difficult to check against other samples.

4 Dijet Analysis

Inclusive dijet production ($pp \rightarrow 2$ jets $+X$) is the dominant LHC process. Simple to observe, and rich in potential signals of new physics, dijets are expected to be one of the earliest CMS measurements. Here we discuss measurement of the cross section versus dijet mass utilizing the single jet triggers defined in the previous section.

4.1 Dijet Mass Analysis

Jets are reconstructed as localized energy depositions in the CMS calorimeters arranged in a projective tower geometry. The jet energy E is defined as the scalar sum of the calorimeter tower energies inside a cone of radius $R = \sqrt{(\Delta\eta)^2 + (\Delta\phi)^2} = 0.5$, centered on the jet direction. The jet momentum $\vec{p}$ is the corresponding vector sum of energies, with the vector pointing in the tower direction. The jet transverse energy is $E_T = E \sin\theta$, and the jet transverse momentum is $p_T = p \sin\theta$, where θ is the angle between the jet momentum and the proton beam. Both the jet energy and momentum are corrected back to the particles in the jet cone originating from the hard interaction excluding pileup, as discussed in section 2. We define the dijet system as the two jets with the highest p_{T} in an event (leading jets) and define the dijet mass $m = \sqrt{(E_1 + E_2)^2 - (\vec{p}_1 + \vec{p}_2)^2}$. We select events in which the leading jets each have $|\eta| < 1$. This cut enhances our sensitivity to new physics, produced at low $|\eta|$, compared to the predominantly t-channel processes from the QCD background. In all plots that are a function of dijet mass, we plot in bins of width equal to the estimated mass resolution [7].

4.2 Rates and Efficiencies from Jet Triggers

We use simulated data from the single jet triggers discussed in section 3. From the three trigger tables for instantaneous luminosities of 10^{32}, 10^{33}, and 10^{34} cm^{-2}s^{-1} we expect initial samples with integrated luminosity of around 100 pb^{-1}, 1 fb^{-1}, and 10 fb^{-1} respectively. This is from 10^6 seconds of collisions, equivalent to one month of continuous operation at 40% efficiency. In Fig. 4 we show the rate expected from these triggers as a function of dijet mass. This was an offline exercise to estimate the rate expected from the triggers. As discussed in section 3 the L1 efficiency is expected to be at least 95% at the p_{T} threshold of the HLT trigger, so it was not necessary to include L1 in these expected rate plots. The turn-on of each trigger in figure 4 is completely due to the difference between the HLT p_{T} threshold listed and the dijet mass variable: we simply plotted the dijet mass distribution of events with a leading jet that passes the p_{T} threshold of the HLT trigger. By construction there are comparable events in each trigger, and a high statistics overlap between triggers for a given table. We note that in this simulation, unlike in the real experiment, a single sample was used to estimate the rate for all the triggers, so the statistics in the overlap regions among the triggers have identical fluctuations: they come from the same sample and are just scaled down in rate by the prescales. We see that the highest mass dijet is expected to be 5, 6 and 7 TeV for samples with integrated luminosity of 100 pb^{-1}, 1 fb^{-1}, and 10 fb^{-1} respectively.

In Fig. 5 we show the trigger efficiency vs. dijet mass and explicitly show the mass cuts that are fully efficient. Here, since we have complete knowledge from the simulation, we simply measured the ratio of triggered events to all events: events with leading jet p_{T} greater than the HLT threshold divided by all events. In the real experiment this efficiency would be measured for each trigger using the neighboring trigger with a lower p_{T} threshold. For example, the trigger efficiency in the *Super* path would be measured by finding the fraction of

events in the *High* path which also satisfied the *Super* trigger. This will allow us to measure the trigger efficiency for all paths except *Low*. If we want to use the *Low* path for physics analysis, we can try and measure its efficiency using any minimum bias trigger samples, if they have sufficient rate. We have conservatively assumed that the *Low* trigger path will not be used for dijet mass physics.

In Fig. 6 we show the data we will use to measure the cross section. We use each trigger where it is fully efficient and stop using the trigger where the next trigger is fully efficient. Fig. 6 shows there are adequate numbers of fully efficient events for analysis. While it is possible to use the overlap among triggers to increase the measurement statistics in the overlap region, in practice this is not done, since the added rate is negligible given the large prescales.

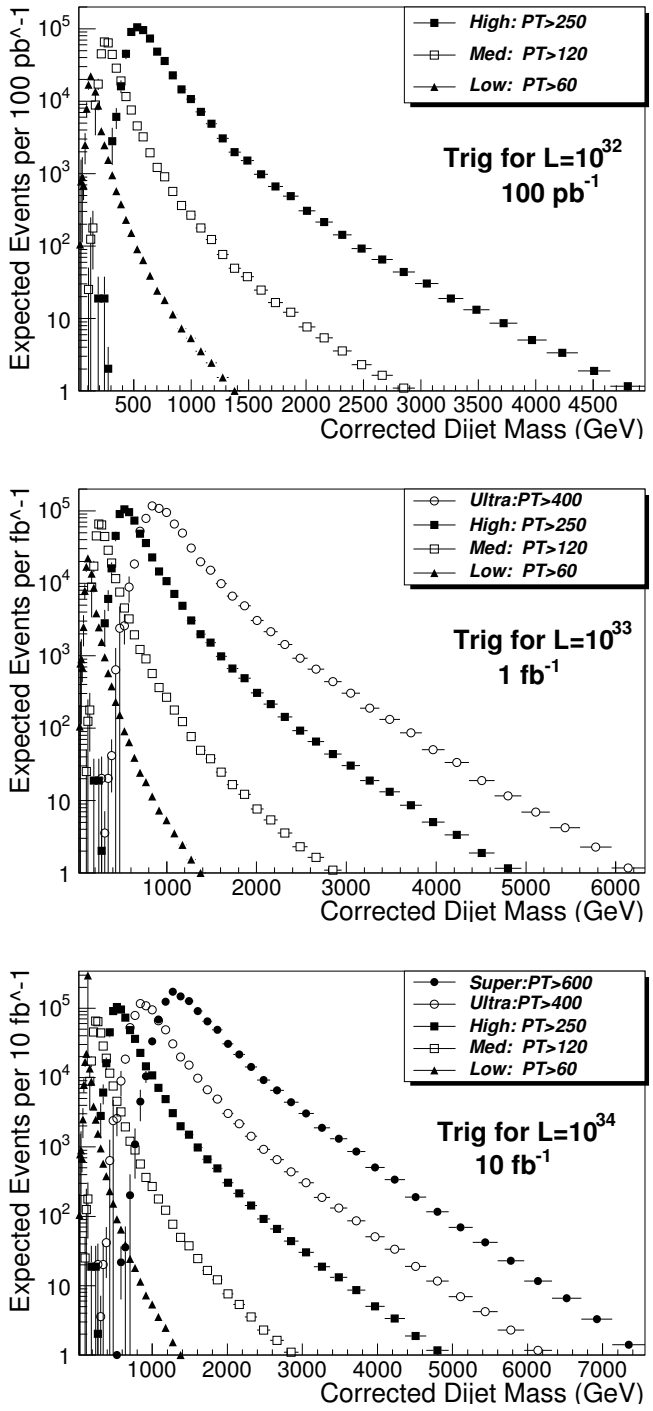

Figure 4: Rate of jet trigger as a function of dijet mass. The 3 plots correspond to 3 luminosity scenarios in the trigger table 1. Each plot shows the rate as a function of dijet mass for multiple triggers with the listed HLT p_{T} thresholds and prescales.

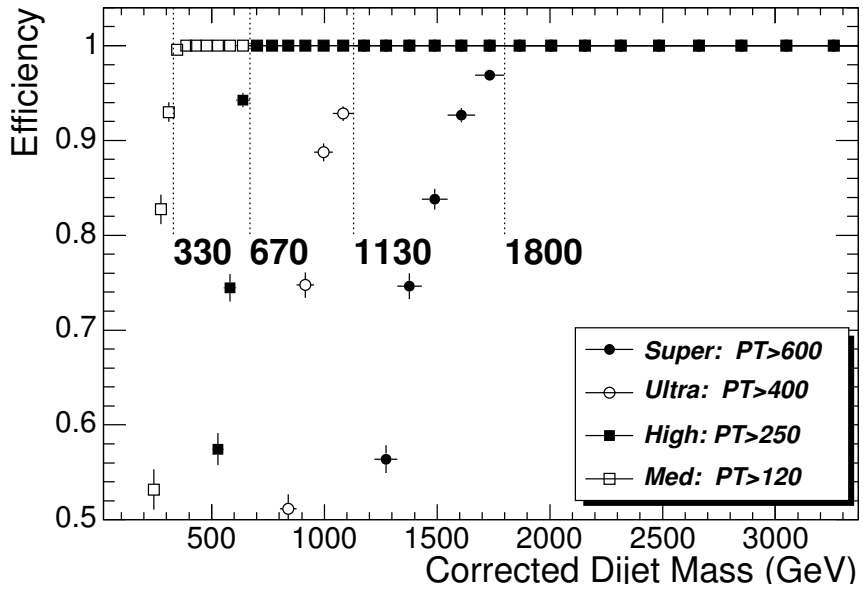

Figure 5: Jet trigger efficiency (points) and fully efficient dijet mass cuts (lines).

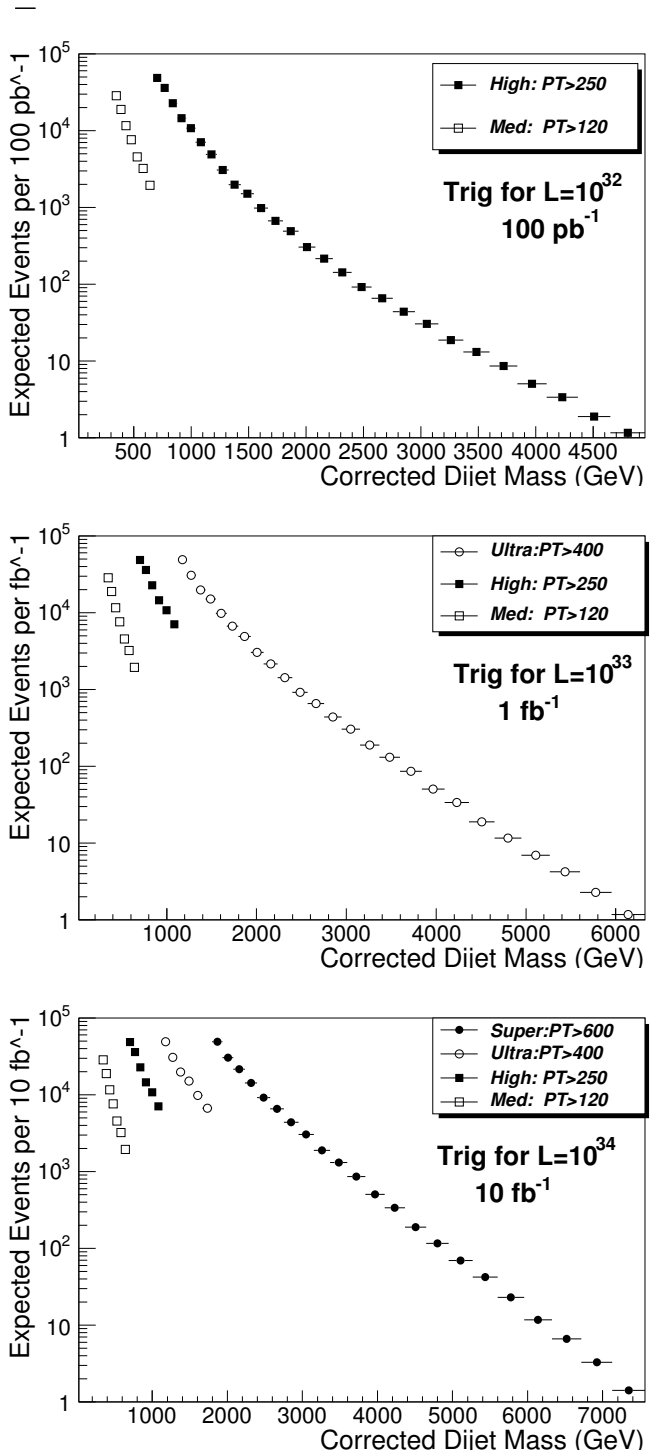

Figure 6: Rate of jet trigger for cross section measurement. Same triggers as Fig. 4 shown here after the dijet mass cuts for full trigger efficiency.

4.3 Dijet Mass Distribution

In Fig. 7 we combine the triggers to produce a differential cross section across the full mass spectrum resulting from QCD dijet production. The prescaled triggers allow us to measure mass down to 330 GeV, or even smaller if we can understand the efficiency of the lowest threshold trigger. The mass measured with the prescaled triggers will allow us to connect to dijet masses measured at the Tevatron [8, 9]. Since there has has been no new physics beyond the standard model discovered in dijets at the Tevatron, this mass region can be a control region of the CMS measurement which defines the QCD background to searches for new physics with dijets.

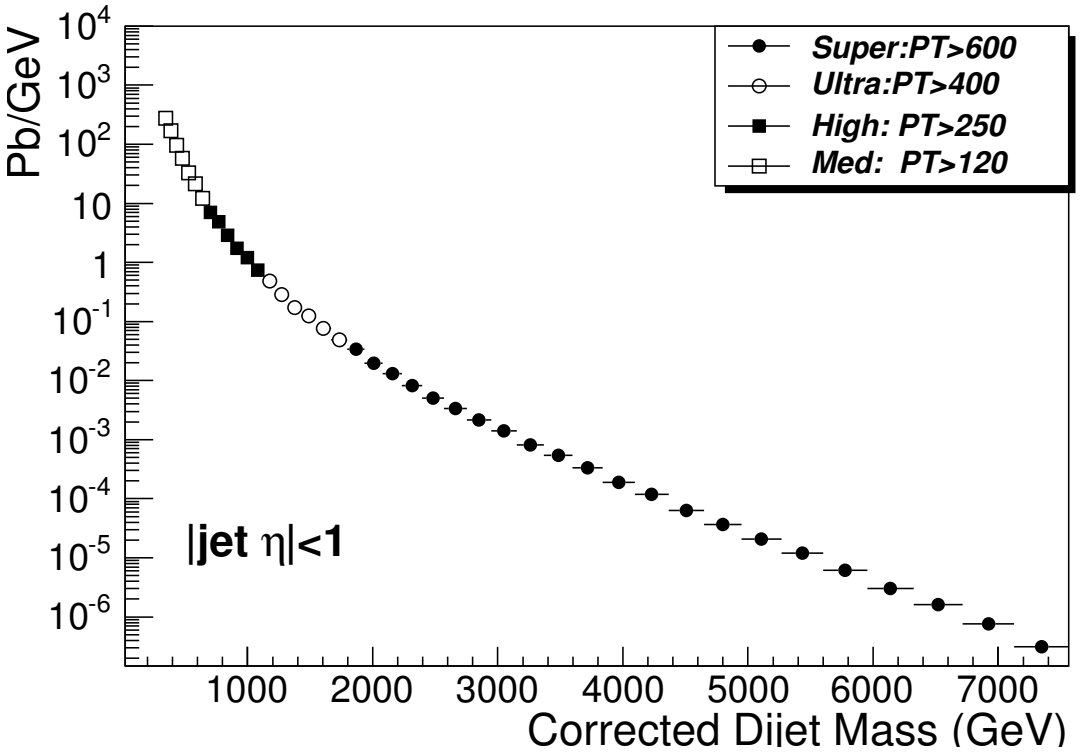

Figure 7: QCD differential cross section vs. dijet mass, showing the contributing jet triggers with different symbols, listed with their path names and p_{T} thresholds at HLT in the legend.

In Fig. 7 the cross sections from each trigger sample trivially combine to form a smooth spectrum, because they all originate from a smooth Monte Carlo distribution. In the actual experiment the data samples come from the different trigger paths of table 1, each with different prescales, and there is always the question of how reliably the paths operated and how well the prescales are known. If the trigger did not always fire when it should, or if the prescales were wrong, then the cross sections from each trigger sample might not combine to form a smooth spectrum, artificially introducing wiggles that could be misinterpreted as new physics. In the real experiment, to insure the integrity of the trigger and prescale, we can measure the cross section in the overlap region where both triggers are fully efficient, and insure that the cross section at a given mass is the same from each trigger. The overlap among triggers was used by the Tevatron experiments [8, 9] to measure the prescales and constrain their systematic uncertainty.

In Fig. 8 we show the fractional statistical error on the cross section, the simplest measure of our sensitivity to new physics. The statistical errors are estimated using Gaussian statistics throughout ($\sigma = \sqrt{n}$). Fig. 8 shows that our prescaled triggers will allow a measurement of QCD with 1-3% statistical accuracy. The unprescaled triggers will have 1% error at threshold and the first unprescaled sample begins at a mass of 670 GeV, giving us full sensitivity to new physics in a region that overlaps with previous dijet mass measurements at the Tevatron [8, 9].

5 Systematic Uncertainties

In figure 9 we summarize our estimates of systematic uncertainties on the dijet cross section. The systematics presented for 1 $\mathrm{fb}^{-1}$are also applicable to 100 pb^{-1}, and an aggresive estimate of systematic uncertainty is presented for 10 fb^{-1}. Our list of systematics is likely incomplete, but we believe the systematics we have estimated will dominate the overall systematic uncertainty on the dijet cross section. The uncertainties presented are discussed in this section.

5.1 Jet Energy

We divide the determination of the jet energy into the determination of two energy scales, also known as two energy multiplication factors, necessary to correct from measured jet energy to true jet energy. The absolute jet energy scale is the energy multiplication factor needed to correct jets constrained to the region $|\eta| < 1$, where the vast majority of energy is measured in the barrel calorimeter. The absolute jet energy scale is a function of p_{T}. The relative jet energy scale is the energy multiplication factor needed to correct jets as a function of η, relative to the region $|\eta| < 1$, and is also a function p_{T}. The relative jet energy scale is a measurement of the uniformity of jet energy response as a function of η. Since our analysis integrates over the region $|\eta| < 1$ only, the relative jet energy scale is not of great importance, and we only discuss it for completeness.

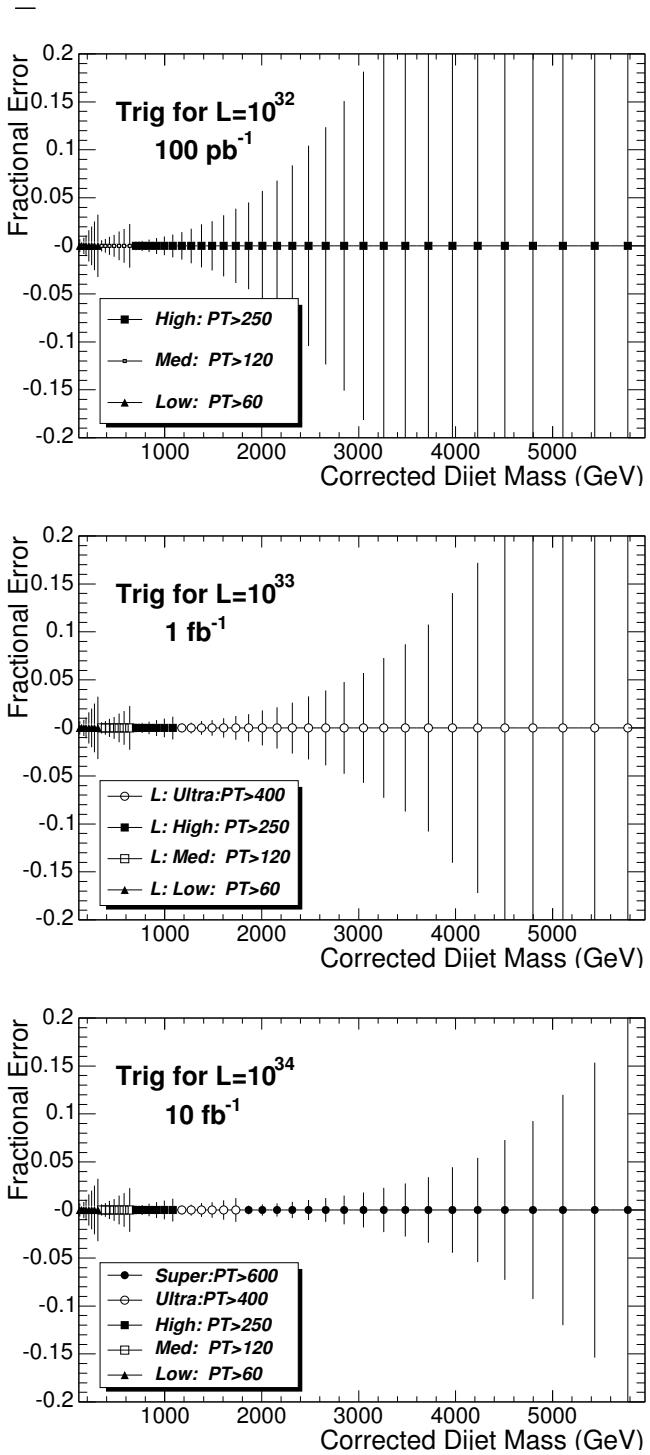

Figure 8: Fractional statistical error on the dijet cross section measured using our proposed triggers.

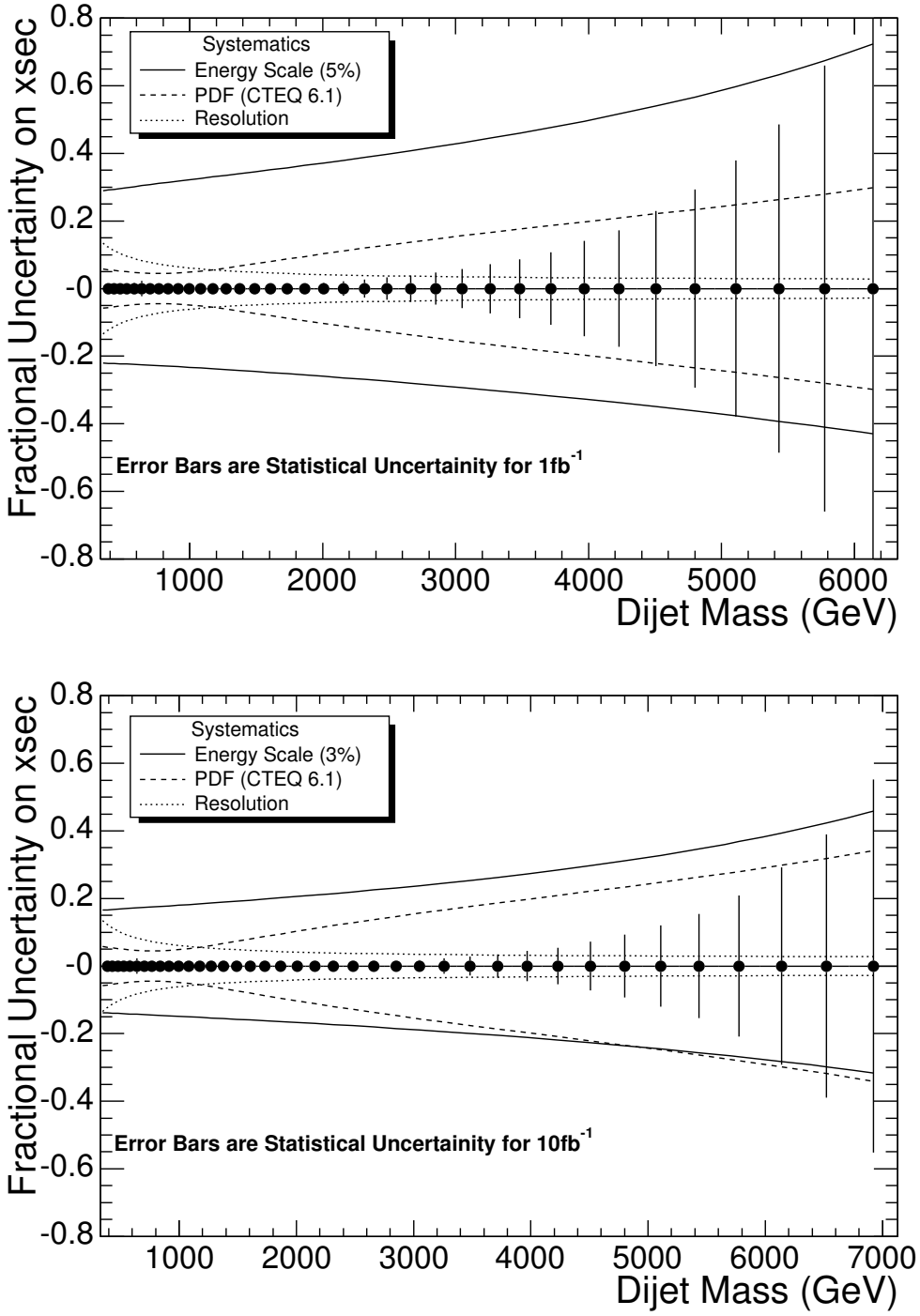

Figure 9: Systematic uncertainty on the dijet cross section due to jet energy scale (solid curve), parton distributions (dashed curve), and calorimeter energy and η resolution (dotted curve) are compared to the statistical uncertainties for 1 fb^{-1}(top plot) and 10 fb^{-1}(bottom plot). For 1 fb^{-1}we assume a jet energy scale uncertainty of 5% and for 10 fb^{-1}a more aggressive estimate of 3% is assumed.

5.1.1 Absolute Jet Energy Scale

Determination of the absolute jet energy scale and its systematic uncertainty is one of the most difficult tasks in hadron collider physics. Following the experience of the Tevatron experiments [10, 11], CMS has adopted a data driven strategy for calibrating the jet energy scale [13] and constraining its uncertainty. We expect that early in the CMS data taking we will determine the jet energy scale from low to moderate jet p_{T} by requiring p_{T} balance in measured photon + jet events [14] and Z + jet events. This technique uses the calibration of the electromagnetic calorimeter, known from Z decays to $e^{+}e^{-}$. To understand the jet energy scale at higher p_{T} than is possible with photon + jet events, we will rely on a Monte Carlo based calibration of the jet energy [2], which relies on a GEANT simulation that has been validated using test beam measurements of charged pions from 5 GeV to 300 GeV [16]. This validation of the simulation will continue using isolated charged tracks measured in the CMS detector, some with p_{T} as high as our test beam measurements, which should allow us to transport the TB high energy pion calibration into the environment of the CMS detector during full operations. Later we will check and improve the jet calibration for quark initiated jets at low p_{T} by constraining dijets to the W mass in events containing a top quark [15].

CMS has concluded that an overall uncertainty on the jet energy scale in the barrel of $\pm 5\%$ is achievable [13] for 1 fb^{-1}. It is likely that the jet energy scale uncertainty will decrease with time. Since the CMS strategy for determining the jet energy scale is similar to that of CDF at the Tevatron, it is reasonable that by the time we have integrated 10 fb^{-1}our systematic uncertainty on the jet energy scale will decrease to roughly $\pm 3\%$ achieved by CDF [10]. We have propogated these energy scale errors to the dijet mass cross section by measuring the effect of these changes in mass on a smooth fit to the dijet mass cross section. The differential cross section is well fit by a simple parameterization of the form

$$\frac{d\sigma}{dm} = \frac{p_0(1 - m/\sqrt{s})^{p_1}}{m^{p_2}} \tag{1}$$

where m is the dijet mass, $\sqrt{s} = 14000$ GeV is the collision energy, and p_0, p_1, p_2 are the fit parameters. Fitting the data in figure 7 from $m = 0.33$ to $m = 7.0$ TeV, gives the fit values $p_0 = 6.3 \times 10^{14}$, $p_1 = 8.0$, $p_2 = 4.8$. Changing m by $\pm 5\%$ in equation 1, and calculating the resulting change in $d\sigma/dm$, gives the fractional uncertainty on the absolute jet energy scale. As shown by the solid curve in the top plot of figure 9, the uncertainty on the cross section varies from +30%(-22%) at a dijet mass of 0.3 TeV/c^2 to +70%(-42%) at a dijet mass of 6 TeV/c^2. For a jet energy systematic of only 3% the uncertainty on the cross section varies from +17%(-14%) at a dijet mass of 0.3 TeV/c^2 to +38%(-28%) at a dijet mass of 6 TeV/c^2. The increase in the fractional uncertainty on the cross section with mass is simply caused by the steepening of the dijet mass spectrum as a function of mass.

5.1.2 Relative Jet Energy Scale

The relative jet energy scale will be determined using dijet balance [17]. In dijet balance one of the two leading jets is required to be in the region $|\eta| < 1$, the other leading jet can be at any η, and the relative jet energy scale is set by requiring that they have equal p_{T} on average. We have shown that by using dijet balance an uncertainty of $\pm 0.5\%$ is achievable [17] for the relative jet energy scale as a function of η within the barrel, in 0.1 steps in η. For the cross section as a function of mass, integrating over the region $|\eta| < 1$, this uncertainty is clearly negligible compared to the $\pm 5\%$ error in the absolute energy scale. We do not consider it further in this analysis.

5.2 Jet Resolution

The effect of calorimeter resolution, in this analysis, is the difference between the measurement with jets constructed from MC particles (Gen Jets) and the measurement with jets constructed from calorimeter depositions and corrected (Rec Jets). This difference, is sometimes called the smearing of the spectrum due to calorimeter resolution. The smearing can be significant, because the steeply falling QCD spectrum combines with a poor measurement resolution for jets, to produce a feed-down effect where many Gen Jets at low mass end up being observed as Rec Jets at high mass. There are simply a lot more Gen Jets at low mass, so even a small probability of them fluctuating to higher mass can produce a large effect. Of course, the magnitude of this smearing is very much coupled to the size of the jet energy corrections themselves, and it is the uncertainty on those jet energy corrections that really dominate the uncertainty in the cross section. Since the problems of resolution uncertainty and energy scale uncertainty are so tightly coupled, and we have already chosen a jet energy correction and assigned it an uncertainty, we have decided to simplify the potentially complicated study of the jet resolution systematic by simply equating it to the uncertainty in the smearing once the jet energy scale has been chosen.

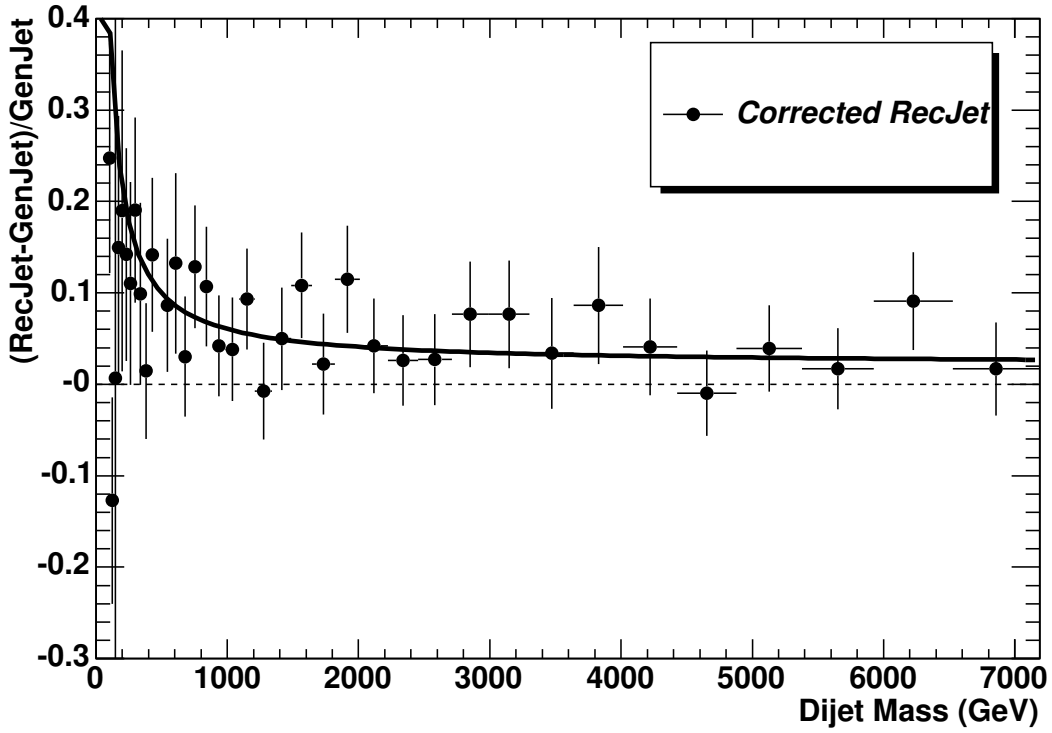

Figure 10: The resolution smearing of the cross section. The fractional difference between the measured dijet cross section in fig. 7 and the MC particle level dijet cross section, is plotted versus corrected dijet mass (points) and fit with a smooth curve.

With this approach, the uncertainty in the smearing is likely bounded by the size of the smearing, or at the very least the uncertainty in the smearing should not be significantly greater than the size of the smearing. In figure 10 we show the resolution smearing as a

function of reconstructed and corrected dijet mass. This is simply the fractional difference between the dijet mass spectrum with corrected Rec Jets and the dijet mass spectrum with Gen Jets. Compared to the jet energy scale uncertainties, the smearing difference between the Rec Jets and Gen Jets spectrum is small. In figure 10 we fit this smearing with a smooth function, and in Figure 9 we show the smooth function as a positive uncertainty and the negative of the smooth function as a negative uncertainty. The positive uncertainty varies from 15% at 0.3 TeV to 3% at 6 TeV,as shown in Figure 9.

5.3 Parton Distributions

Uncertainties in parton distributions produce uncertainties in theoretical predictions of the QCD cross section as a function of dijet mass. When the dijet mass distribution is measured, we will compare it to the QCD prediction, and this uncertainty in the theory will make the search for new physics more difficult. Therefore, although this uncertainty does not affect our future measurement, it can affect our future search for new physics, and so we consider it here.

Previous experiments colliding hadrons with various targets provide information on Parton Distribution Functions (PDFs) that can be evolved to LHC energies. Attempts to extract the PDFs are affected by uncertainties in the experimental measurements and the theory that describes them. The CTEQ collaboration provides a PDF set which includes both the best fit PDF and the errors resulting from the fit between world data and theory [18]. We have used CTEQ 6.1, which has 40 different error PDFs: 20 PDFs at positive error (S_i^+), and 20 PDFs at negative error (S_i^-). They recommend that the error on any observable quantity, X, be calculated using the formula

$$\Delta X = \frac{1}{2}\left(\sum_{i=1}^{20}\left[X(S_i^+) - X(S_i^-)\right]^2\right)^{1/2}, \tag{2}$$

This requires the user to explicitly calculate the observable quantity 40 times in order to calculate the error ΔX. This can be a prohibitively large task for a Monte Carlo and detector simulation. Instead, to simplify the problem ,we have used our own lowest order analytic calculation of the differential cross section versus dijet mass. This is sufficient to determine uncertainties due to parton distributions for this analysis since our lowest order calculation makes the same use of the parton distributions as does the Pythia Monte Carlo. For each bin of dijet mass we calculated the lowest order cross section in that bin, $d\sigma/dm$, using the default CTEQ6.1 set, and then used equation 2 to calculate the uncertainty in the cross section, $\Delta d\sigma/dm$. As shown in figure 9, the resulting fractional uncertainty in the differential cross section varies from 5% at a dijet mass of 0.3 TeV to 29% at a dijet mass of 6 TeV.

5.4 Luminosity, Efficiency and Acceptance

To the best of our knowledge there has been no CMS study of what uncertainty we can expect in the measurement of the LHC luminosity. We therefore do not present an estimate for it in Figure 9. Nevertheless, from the prior experience of the Tevatron, where the luminosity was measured via the total $p\bar{p}$ scattering cross section, we could expect the uncertainty in the luminosity to be of order 10%. It is possible that the W or Z cross section might be more appropriate for a luminosity measurement. If the luminosity at CMS were measured via simply measuring either the W or Z rates in a lepton decay channel, and dividing by the theoretical cross section, we might expect of order 10% theoretical uncertainty in the NLO

cross section and of order 10% experimental uncertainty in the measurement, leading to an uncertainty of order 10% in the luminosity.

Efficiency is not an issue, since at dijet masses greater than $0.33\ \mathrm{TeV}/c^2$ there is full efficiency for finding a dijet in the region $|\eta| < 1$ with negligible uncertainty. Acceptance is also not an issue, since our acceptance for the two leading jets is defined by our cut at $|\eta| < 1$. Any measurements made with an $|\eta| < 1$ cut must be compared to theoretical predications that also have an $|\eta| < 1$ cut. There is negligible uncertainty in the relative acceptance of the measured and calculated jet η region.

6 Conclusions

We have proposed a table of single jet triggers for CMS. The trigger table includes p_{T} thresholds, prescales, and rate estimates at L1 and HLT for four luminosities: 10^{32}, 10^{33}, 2×10^{33} and 10^{34} $\mathrm{cm}^{-2}\mathrm{s}^{-1}$. The trigger is primarily constrained by the allowed HLT bandwidth for jets, which then defines the threshold of the highest E_{T} jet trigger which must not be prescaled. The L1 threshold can then be chosen at a low enough value so that there is full L1 efficiency at the HLT threshold, a luxury we could not afford at the Tevatron.

In the design of the trigger table we have been guided by both Tevatron experience and the concerns of subsequent jet analysis. The triggers are organized in paths, where the HLT trigger in the path only considers events coming from the L1 trigger in the path. To facilitate the combination of trigger samples across the years, the trigger prescales are increased with increasing luminosity, but E_{T} thresholds in the trigger are never changed. New E_{T} thresholds without any prescale clearly must be added at large jumps in the luminosity of the LHC, but these thresholds remain permanently thereafter for continuity of analysis. The thresholds have been chosen to provide data at low enough dijet mass to significantly overlap with the Tevatron measurements, which serve as a control region for the search for new physics.

We have presented an analysis of the dijet mass distribution from QCD that would result from the proposed trigger table. To facilitate searches for new physics on this background we have constrained the two leading jets to each have $|\eta| < 1$. We have presented the dijet mass thresholds where our single jet trigger is fully efficient. QCD events can be analyzed from a lowest dijet mass of 0.3 TeV to the highest dijet mass expected, which is around 5 TeV for 100 pb^{-1}, 6 TeV for 1 fb^{-1}, and 7 TeV for 10 fb^{-1}. We have shown that the triggers will have both sufficient overlap and adequate numbers of events for analysis. The statistical uncertainty in a bin of dijet mass at threshold will be better than 1%, increasing to 3% just before the next trigger is used.

We have made some initial estimates of the significant systematic uncertainties in the dijet cross section. Experimental uncertainties are dominated by an estimated 5% uncertainty in the jet energy scale, which produces an uncertainty in the differential cross section between 30% and 80% as a function of dijet mass. Theoretical uncertainties in the parton distributions are smaller, but non-negligible.

This proposed trigger and dijet analysis are the foundation of CMS preparations to search for dijet resonances [7] and quark contact interactions [19]. We hope it will also stimulate further work to prepare the trigger and jet analysis at CMS.

A References

[1] ORCA 8_7_3 at http://cmsdoc.cern.ch/ORCA/.

[2] A. Heister, O. Kodolova, V. Konoplianikov, S. Petrushanko, J. Rohlf, C. Tully, A. Ulyanov, *"Measurement of Jets with the CMS Detector at the LHC"*., **CMS NOTE-2006/036**.

[3] The RecJetRootTree code is in the ORCA 8_7_1 package at [1].

[4] R. Demina, J. Dolen, C. Justus, P. Tipton, M. Zielinski, R. Harris, *Calorimeter Cell Energy Thresholds for Jet Reconstruction in CMS*, **CMS NOTE-2006/020**.

[5] The JetMET root tree code is in the ORCA 8_7_3 package at [1].

[6] Fredrik Oljemark and Monika Grothe, private communications on April 19-20, 2005.

[7] K. Gumus, N. Akchurin, S. Esen and R. Harris, *CMS Sensitivity to Dijet Resonances*, **CMS NOTE-2006/070**.

[8] CDF Collaboration (T. Affolder et al.), a measurement of the differential dijet mass cross-section in p anti-p collisions at $\sqrt{s} = 1.8$ TeV, Phys.Rev.D61:091101 (2000), hep-ex/9912022.

[9] D0 Collaboration (B. Abbott et al.), the dijet mass spectrum and a search for quark compositeness in anti-p p collisions at $\sqrt{s} = 1.8$ TeV, Phys.Rev.Lett.82:2457-2462 (1999), hep-ex/9807014.

[10] A. Bhatti et al., *Determination of the jet energy scale at the collider detector at fermilab*, FERMILAB-PUB-05-470, October 2005, hep-ex/0510047.

[11] D0 Collaboration, B. Abbott et al., *Determination of the absolute jet energy scale in the D0 calorimeters* Nucl. Instrum. and Methods A424 (1999) 352-394, hep-ex/9805009.

[12] CMS Collaboration, D. Acosta et al., **CMS Physics TDR Volume 1**, CERN/LHCC 2006-001 (2006).

[13] PTDR1 [12], Section 11.6.1: *Data-driven calibration strategy* beginning on page 421.

[14] PTDR1 [12], Section 11.6.3: γ + *jet events* beginning on page 423. Also V. Konoplianikov, A. Ulyanov, O. Kodolova, *Jet Calibration using γ + Jet Events in the CMS detector.*, **CMS NOTE-2006/042**.

[15] PTDR1 [12], Section 11.6.5:*Jet energy scale calibration using the W boson mass constraint in top quark events* beginning on page 428. Also J. D'Hondt, S. Lowette, J. Heyninck, S. Kasselmann, *Light quark jet energy scale calibration using the W mass constraint in single-leptonic $t\bar{t}$ events*, **CMS NOTE-2006/025**.

[16] PTDR1 [12], Section 5.4: *HCAL performance in test beams* page 216-224. Also, V. Daniel Elvira, *Validation of Geant4 Physics Using the CMS HCAL Test Beam 2002 Experiment*, **CMS NOTE-2004/021**.

[17] PTDR1 [12], Section 11.6.2: *Dijet Balancing* beginning on page 422.

[18] J. Pumplin et al., *New generation of parton distributions with uncertainties from global QCD analysis*, JHEP 07 (2002) 012, hep-ph/0201195.

[19] S. Esen and R. Harris, *CMS Sensitivity to Quark Contact Interactions using Dijets*, **CMS NOTE-2006/071**.